Supporting Information

Novel Preparation of zinc ferrite nanoparticles and performance study of photocatalytic reduction of U(VI)

S1. Experimental reagents

Zinc chloride, ferric chloride, sodium hydroxide, sodium carbonate, nitric acid and hydrochloric acid are purchased from Xilong Chemical Co.Methanol, anhydrous ethanol, azoarsine III, tert-butyl alcohol and chloroacetic acid were purchased from Shanghai Aladdin Reagent Co.All chemicals were obtained from commercial suppliers and used without further purification. The uranium solution used in the experiment is obtained by dissolving $UO_2(NO_3)_2 \cdot 6H_2O$ in mixture of 10 $mmol \cdot L^{-1}$ $NaHCO_3$ aqueous solution.

S2. Material Characterization Methods

S2.1. X-ray powder diffractometer (XRD)

The physical structure of the sample was analyzed by Bruker D8 Advance XRD. The crystal structure of the powder was studied by X-ray diffraction with Cu Kα radiation at an accelerating voltage of 40 kV and an applied current of 40 mA at a scan rate of 0.1° 2θ s^{-1}, and effective crystal parameters were obtained by scanning in the range of 5 to 80°.

S2.2. Laser Raman Spectroscopy (Raman)

The Raman spectra of the samples were obtained using a LabRAM HR laser Raman spectrometer with a laser wavelength of 473 nm and an excitation range of 100-1000 cm^{-1}.

S2.3. X-ray photoelectron spectroscopy (XPS)

The x-ray photoelectron spectra of the material surface were measured by ESCALAB 250xi XPS to characterize the chemical morphology and molecular structure of the material surface, while the valence band potential information of the material was obtained by XPS-VB test. The model of XPS instrument is Shimadzu AXIS SUPRA+. The ion gun emits ion beam on the material, the ion gun voltage is 1EV-5000EV, and the X-ray beam size is less than 10 μm. Imaging resolution should be less than 3 μm (actual measurement 1.49 μm) and chemical state imaging resolution should be less than 1 μm (actual measurement 0.836 μm), the full spectrum difference is 1eV, the fine spectrum difference is 0.1 eV, the dwell time is 300ms, and the passing energy is 40 eV.

S2.4. Field emission scanning electron microscopy (SEM)

The apparent morphological structure of the material was characterized by using JSM-7900F SEM, and the elemental distribution on the surface of the material was observed and analyzed by the accompanying EDS (Model is OXFORD Xplore) energy spectrometer.The working distance of energy spectrum analysis is 8.5mm, the acceleration voltage is 0.02-30kV, the probe beam current is 3pA-20nA, and the electron beam in the mirror tube has no cross optical path.

S2.5. Transmission Electron Microscopy (TEM)

The microstructure of the samples was further investigated using Thermo Fisher Apreo TEM for effective analysis of the particle size and lattice distribution. The overall elemental composition of the material was analyzed using a paired EDS energy spectrometer.

S2.6. Zeta potential

Ten mg of the sample was weighed and ultrasonically dispersed in 50 ml of deionized water, and the solution was adjusted to pH 2 with 1 mol-L^{-1} HNO_3 . Potentiometric measurements were performed with a LAMBDA 950 analyzer in the pH

range of 2-8.

S2.7. Ultraviolet diffuse reflectance spectroscopy (UV-vis DRS)

The UV-Vis spectrum of the material was tested using a T10 UV-Vis spectrophotometer with barium sulfate powder as the reflectance standard.

S2.8. Electrochemical performance testing

Electrochemical tests such as electrochemical impedance (EIS), transient photocurrent (TPCR), and Mott-Schottky (M-S) curves was measured in a conventional three-electrode configuration by an electrochemical analyzer CHI 660D electrochemical workstation (Chen Hua, Shanghai, China). More specifically, a three-electrode system consisting of 0.1 mol/L potassium ferricyanide and 0.1 mol/L potassium chloride as the electrolyte, a platinum wire electrode as the counter electrode, an Ag/AgCl electrode as the reference electrode, and a glassy carbon electrode as the working electrode was used for the EIS and M-S curves. The working electrode was prepared as follows: 1 mg of sample was ultrasonically dispersed in 1 ml of deionized water to prepare a suspension. A small amount of the suspension was taken on the surface of the glassy carbon electrode and then the glassy carbon electrode covered with the sample was dried in an oven and repeated several times. The transient photocurrent test was performed with 0.5 mol/L Na_2SO_4 aqueous solution as the electrolyte and 300 W xenon lamp as the light source, and the light/light avoidance treatment was performed at certain time intervals during the test.

S2.9.Temperature-dependent PL spectrum

The temperature-dependent PL spectrum instrument is composed of sample table, fluorescence emitter, liquid nitrogen constant temperature controller and fluorescence receiver. The sample was filled with sample tank, pressed with slide, and then the sample table was placed in the instrument, so that the fluorescence emission port was aligned with the sample tank. The liquid nitrogen constant temperature controller t was turned on, and liquid nitrogen was added to the sample table. The fluorescence data of the samples at different low temperatures were measured successively.

S3. Photocatalytic performance test

Photocatalytic U(VI) removal experiments were performed in a quartz reactor with circulating condensate at 25 ± 0.2 °C and a xenon lamp with a 420 nm cutoff filter at 300 W. The photocatalytic reaction was performed with a standard solution of uranium at a concentration of 100.0 mg/L. The uranium standard solution used for the photocatalytic reaction was 100.0 mg/L. The uranium standard solution was adjusted to the appropriate pH with nitric acid (HNO_3) and sodium carbonate (Na_2CO_3) solutions. To 50 mL of uranium standard solution adjusted to the corresponding corresponding pH, 10 mg of photocatalyst powder was added and 2 mL of methanol was added as a cavity sacrificial agent. The suspension containing the photocatalyst needs to be stirred for 180 min under dark conditions before the light illumination to reach the adsorption-desorption equilibrium of U(VI) on the surface of the photocatalyst. At each stage of the experimental reaction, 1 mL of the reaction suspension was taken at intervals and the solids were removed by filtration through a 0.22 um nylon syringe, and the U(VI) was determined spectrophotometrically by arsenazo-III. The concentration of U(VI) was determined by arsenazo-III spectrophotometry. The removal rate X of U(VI) was calculated by equation 2.1.

$$X=\frac{C_0-C_t}{C_0}\times 100\% \tag{2.1}$$

where C_0 and C_t are the concentration of U(VI) in the initial solution and the concentration of U(VI) in the solution after the reaction time t, respectively; the photocatalytic rate R_V is calculated by Equation 2.2 .

$$R_V=\frac{1000XC_0V}{238MT} \tag{2.2}$$

where X is the U(VI) removal rate after a certain time of light irradiation (X=0~100%); C_0 is the initial concentration of U(VI) solution in mg/L; V is the volume of solution in L; M is the mass of photocatalyst in g; T is the irradiation time in h; 1000 is a constant and 238 is the molecular weight of uranium. In the active species capture experiments, 2 mL of methanol was replaced with 2 mg of p-benzoquinone (p-BQ) and

2 mL of tert-butanol (TBA), both of which were used as sacrificial agents for -O_2^- and -OH, respectively. In the cycling experiments, the recovered catalysts were soaked in 1 mol-L^{-1} of Na_2 CO_3 solution to elute the uranium deposited on the catalysts, washed with deionized water to neutral and then dried for the next cycling experiment.

S4. Characterization and analysis

The ferrite materials with different Zn/Fe ratios were characterized by HRTEM. Firstly, only the lattice spacing of Fe_2O_3 is observed in the (110) and (202) crystal planes, and with the introduction of Zn, the product at this time behaves as $Z_{0.25}FO$. Gradually, $ZnFe_2O_4$ appears in the HRTEM images, first in the (222) and (331) crystal planes, while there is still Fe_2O_3 present in the product due to the excess of Zn, i.e., (021) and (104) When the ZnFe ratio is flat, the product is ZFO, and only $ZnFe_2O_4$ is present in the image at this time,0.488 nm, 0.301 nm, 0.256 nm, 0.211 nm and 0.163 nm are observed on the ZnFe2O4 (111), (220), (311), (400) and (511) crystal planes, respectively. nm and 0.163 nm lattice stripes. When the Zn content continues to increase to excess, the product behaves as Z_2FO, and three different crystalline facets of ZnO can be observed in the images in addition to $ZnFe_2O_4$. (100), (110) and (102) crystalline facets of ZnO confirm the appearance of ZnO crystalline phase in the Z_2FO material. The results of the four HRTEM images are consistent with the XRD results. In combination with these results, nano-Fe_2O_3 and $ZnFe_2O_4$ were successfully synthesized. The crystalline phase of zinc ferrite with different ZnFe ratios was examined by XRD, and the synthesized Fe_2O_3 (Z_0FO) showed obvious characteristic peaks, and with the addition of zinc, the characteristic peaks belonging to $ZnFe_2O_4$ were obvious until finally the characteristic peaks of ZnO appeared, and there were no spurious peaks nor new characteristic peaks, which indicated that the ZnFe ratio was in a wide range, and the zinc ferrite materials all existed in the form of $ZnFe_2O_4$. Further analysis of the chemical structure of zinc ferrite using XPS demonstrated the presence of trivalent iron ions and zinc ions, indicating that the introduction of zinc induces the presence of Fe in the form of Fe^{3+}. The morphological changes observed using SEM revealed that small particles on nanoparticles started to deposit on the surface of larger

particles, while EDS illustrated that $ZnFe_2O_4$ could exist in the form of $ZnFe_2O_4$ in the range of 0.22 to 0.80 for both Zn-Fe ratios.

S5. Optical performance analysis

A series of photocurrent performance studies were conducted to further investigate the reasons for the improved performance of ZFO photocatalysts for photocatalytic U(VI) removal under low light conditions. The photocurrent response intensity of the ZxFO photocatalyst was reflected by testing the photocurrent of the photocatalyst under short-period light and dark, 20 s period light/light avoidance conditions as a function of light time. With the increase of Zn content, the current change in the Z0.5FO material was delayed, but the current under light was slowly enhanced, indicating that the photogenerated carriers of the material became more and the photoresponse was enhanced.

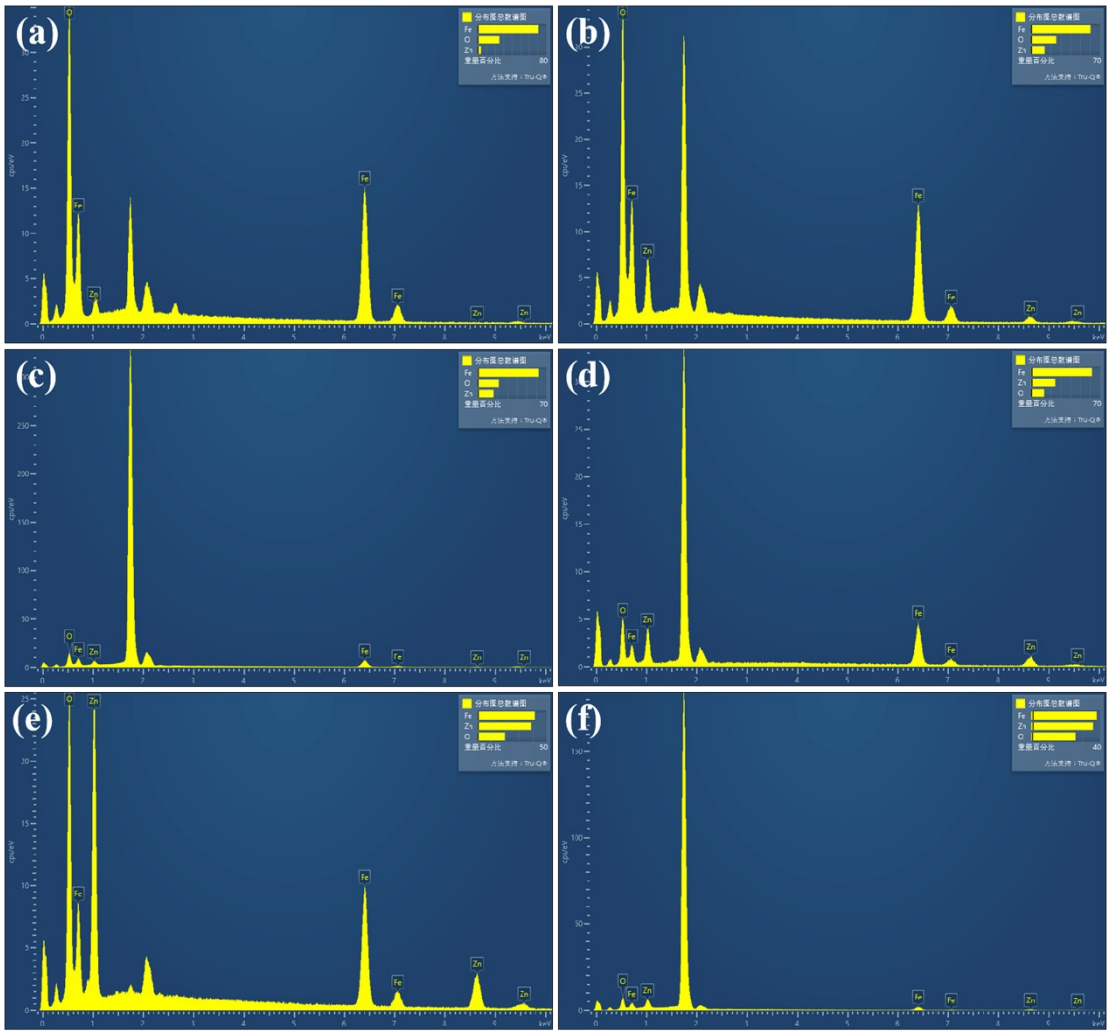

Fig. S1. The elemental mapping images of Z_xFO (a) Fe_2O_3 (Z_0FO); (b) $Z_{0.25}FO$; (c) $Z_{0.5}FO$; (d) ZFO; (e) $Z_{1.5}FO$; (f) Z_2FO

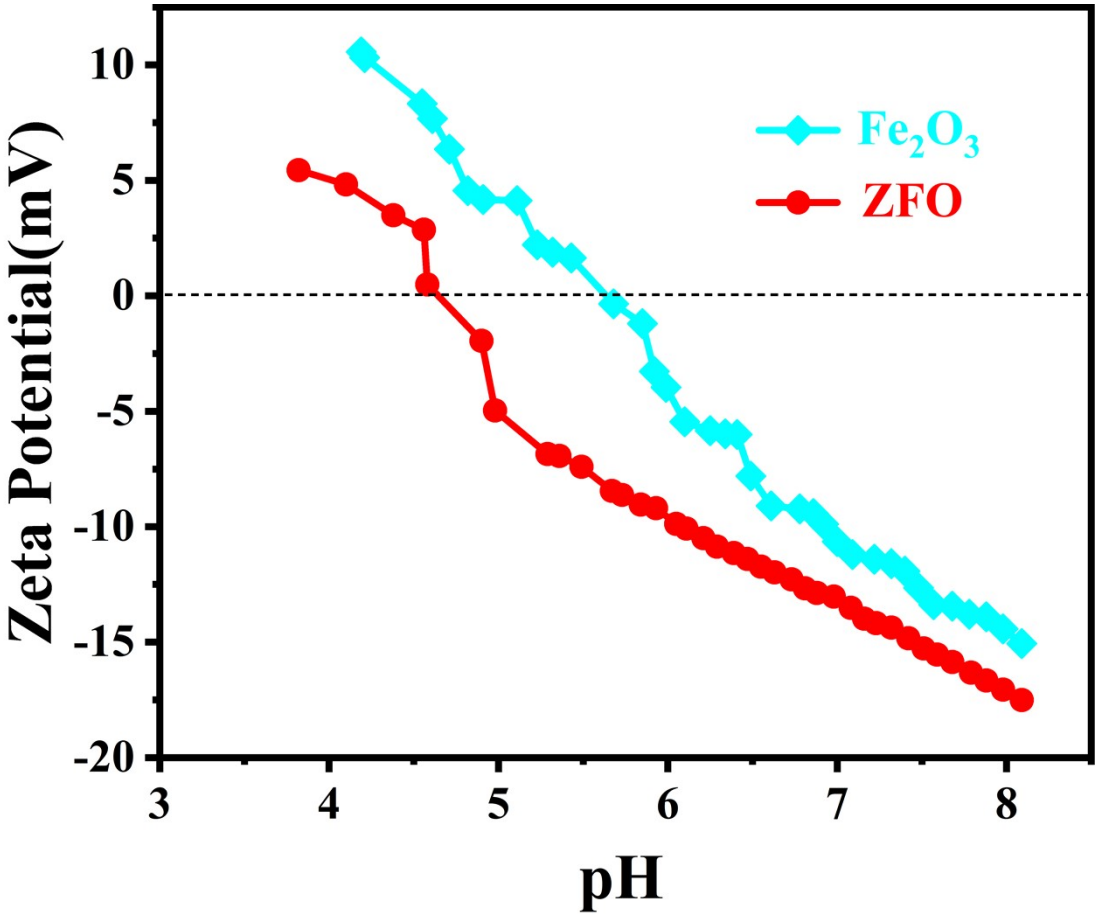

Fig. S2. The Zeta potential of Fe_2O_3 (Z_0FO) and ZFO

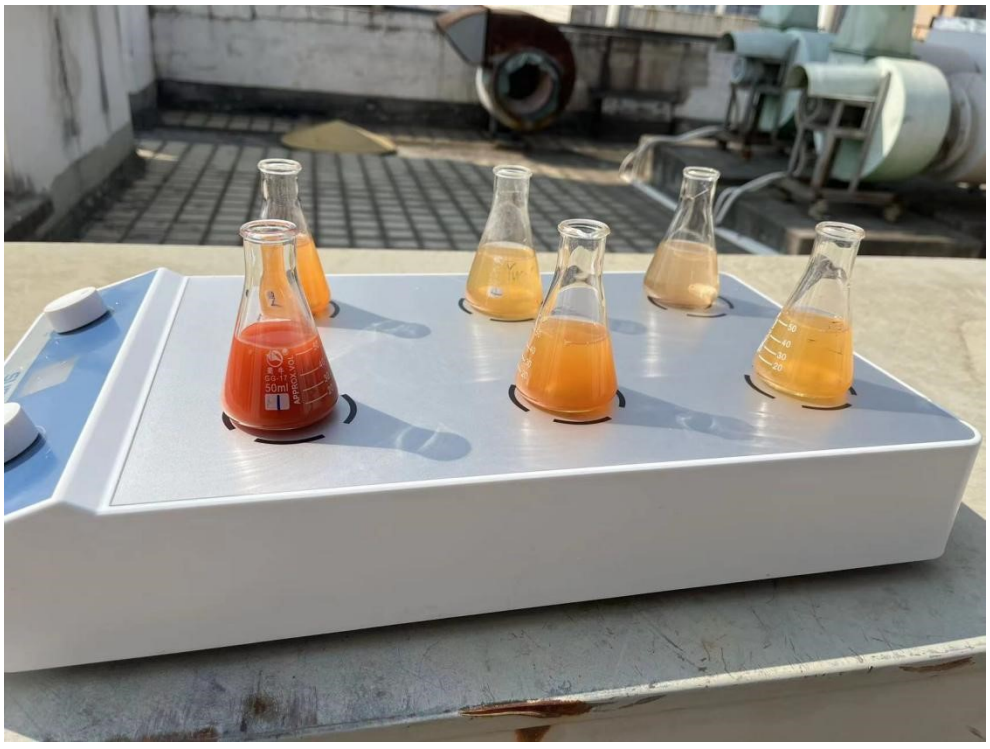

Fig.S3. Schematic diagram of the photocatalytic device under natural conditions

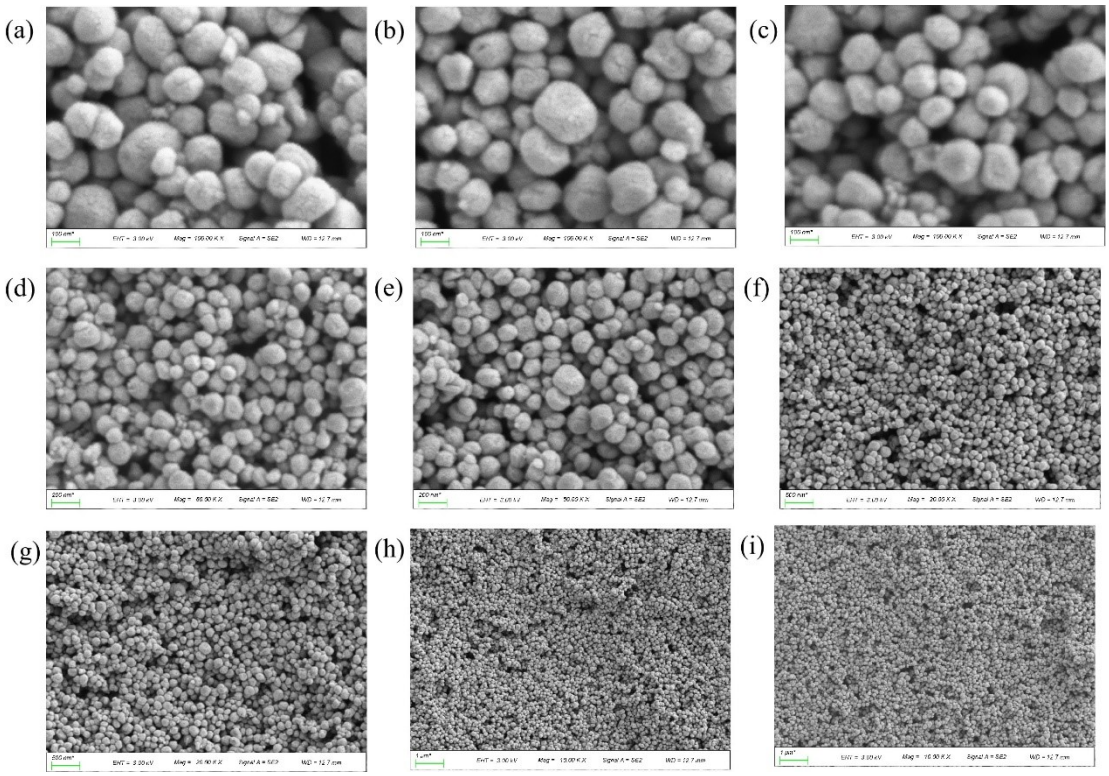

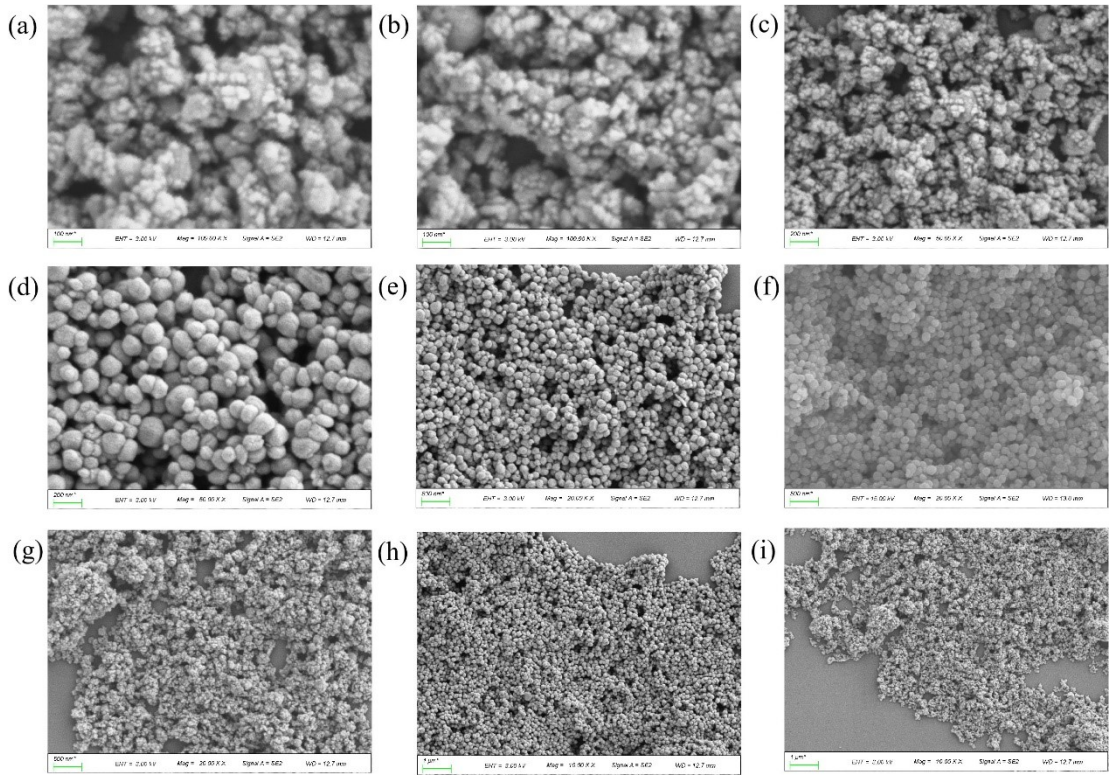

Fig.S4. The SEM images of Z_xFO

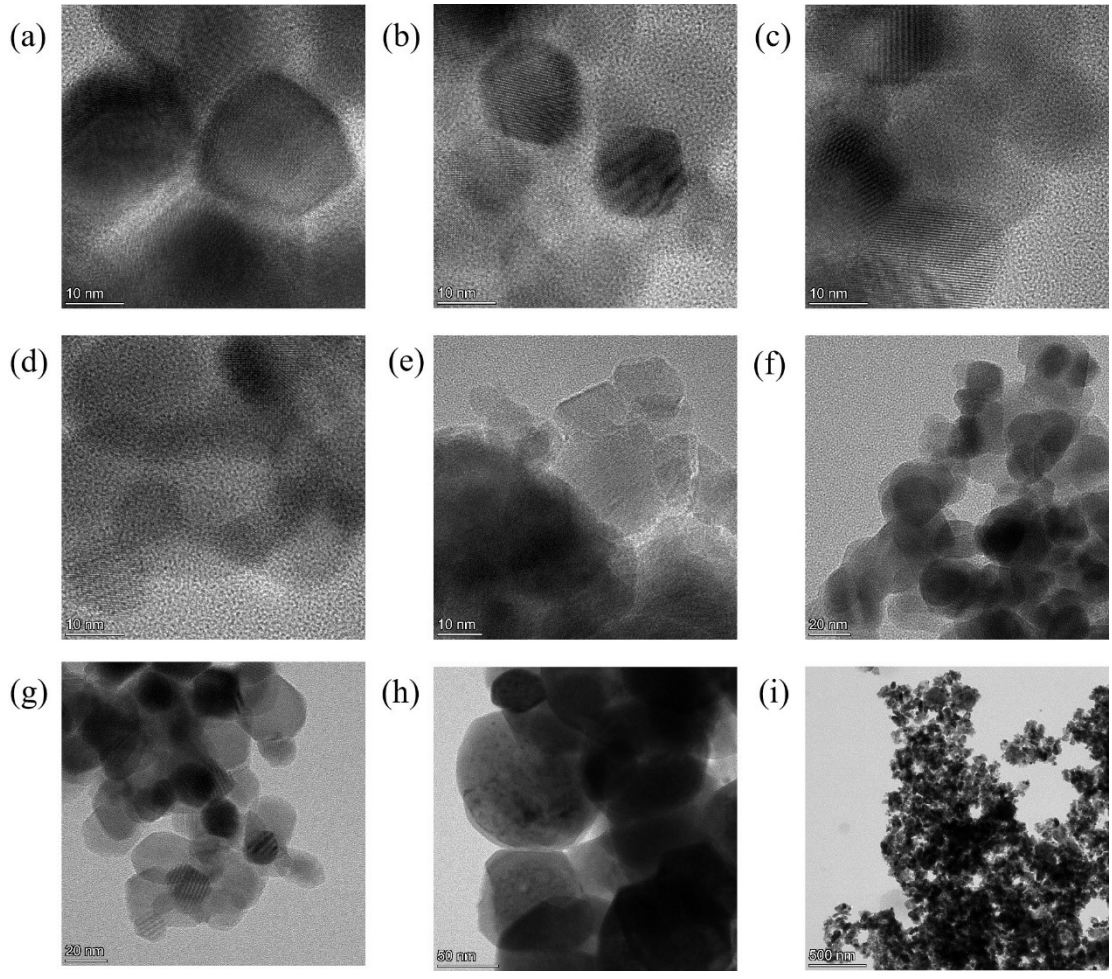

Fig.S5. The HRTEM images of Z_xFO

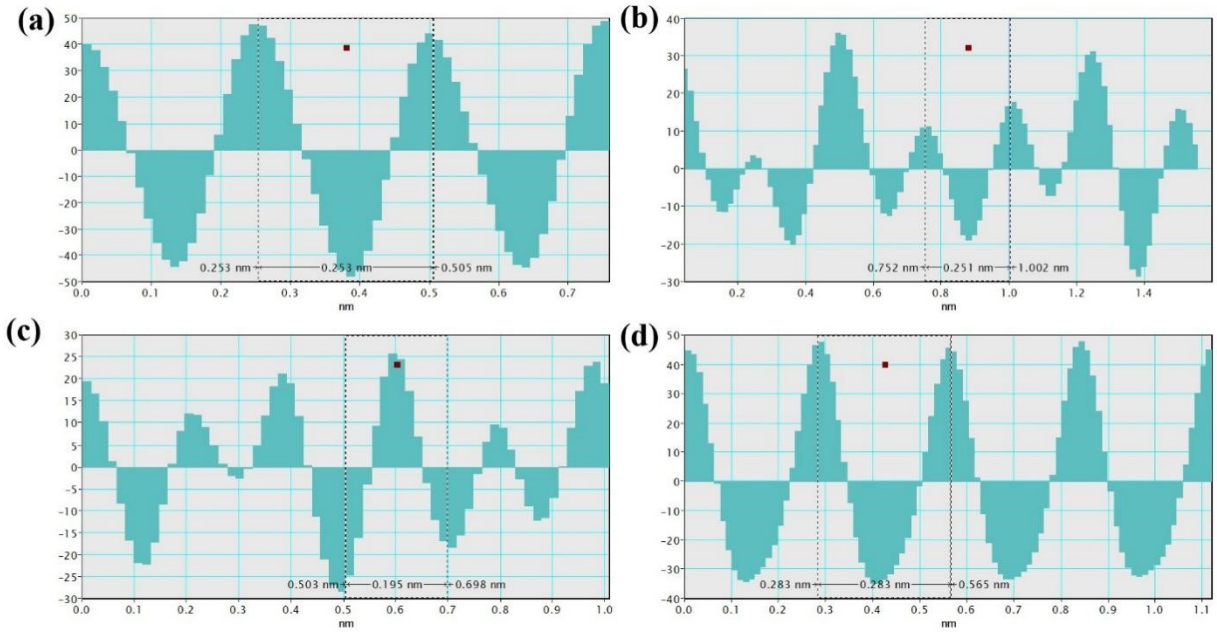

Fig. S6. The lattice spacing of (a) (110) Crystal plane Fe_2O_3. (b) (222) Crystal plane ZFO. (c) (331) Crystal plane ZFO. (d) (100) Crystal plane ZnO.

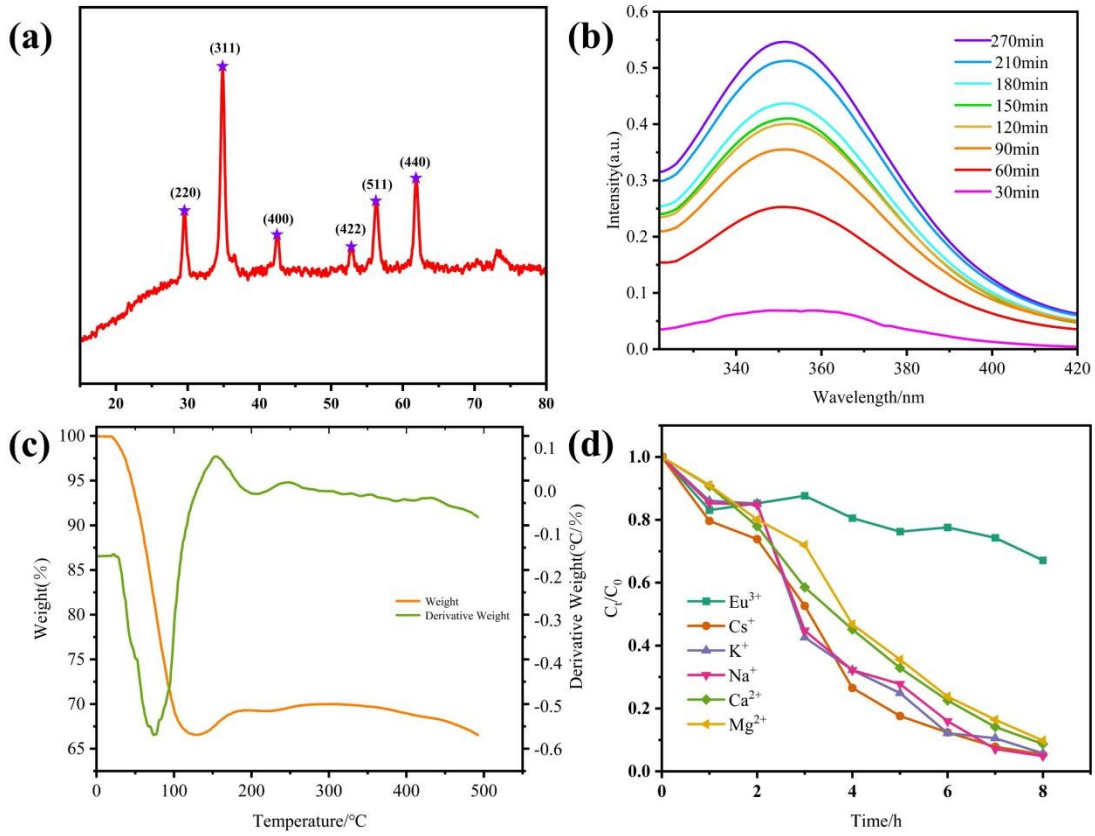

Fig. S7. (a) xrd image of $ZnFe_2O_4$ after photocatalytic reaction. (b) Experiment of H_2O_2

production by ZFO. (c) TGA image of ZFO. (d) ZFO metal ion competition experiment.

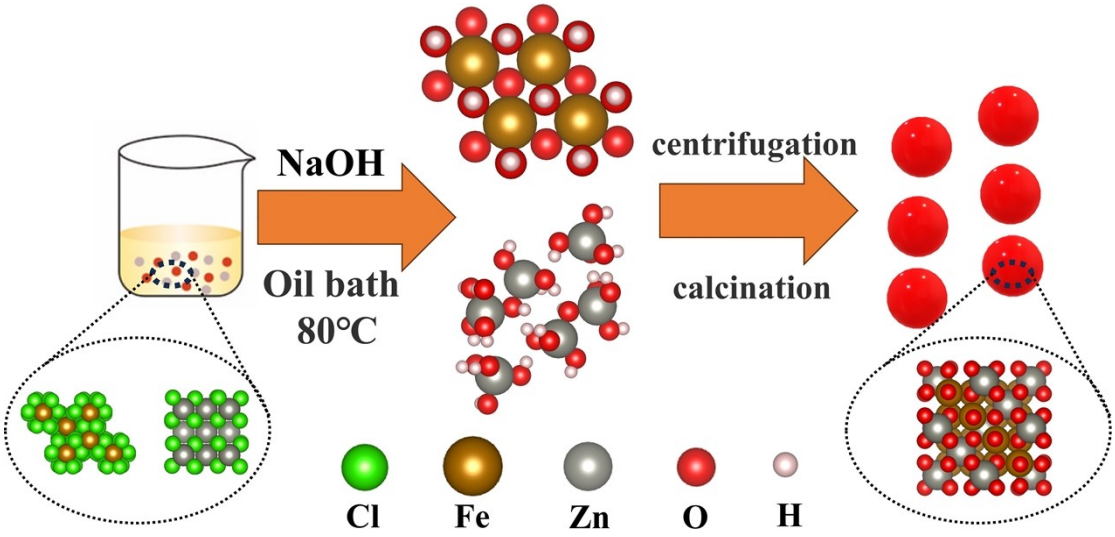

Fig. S8. ZFO synthesis process diagram.